PCCP

PAPER

Cite this: *Phys. Chem. Chem. Phys.*, 2018, **20**, 21313

Dynamic heterogeneity in aqueous ionic solutions†

Gan Ren,[a] Lin Chen[b] and Yanting Wang*[cd]

It is well known that supercooled liquids have heterogeneous dynamics, but it is still unclear whether dynamic heterogeneity also exists in aqueous ionic solutions at room or even higher temperatures. In this work, taking KSCN aqueous solutions as an example, we identify by molecular dynamics simulation that dynamics of ionic solutions at a finite concentration are heterogeneous at room and even higher temperatures. Our results indicate that thermal movements of K^+ and SCN^- deviate from the Gaussian distribution in time and space, as demonstrated by a non-Gaussian parameter and the self-van Hove function. The dynamic susceptibility is nonzero at intermediate times for both K^+ and SCN^-. The self-intermediate scattering function of ions decays in a stretched exponential way with an exponent smaller than one. The dynamics of the solution are more homogeneous at a higher temperature. Since transient ion clusters of different sizes decay with different lifetimes and exponents, we propose that the dynamic heterogeneity is introduced by transient cluster formation and dissociation in ionic solutions, which leads to a mixed relaxation scenario. Variants of the Stokes–Einstein relation are found to break down into a fractional form analogous to supercooled liquids, but the original Stokes–Einstein relation is indeed valid if taking into account the temperature dependence of the effective hydrodynamic radius. Overall, despite some quantitative differences, the dynamic heterogeneity in aqueous ionic solutions at room or higher temperatures is qualitatively analogous to that in supercooled liquids at a much lower temperature.

Received 2nd May 2018,
Accepted 30th July 2018

DOI: 10.1039/c8cp02787k

rsc.li/pccp

1 Introduction

Aqueous ionic solutions have wide application in many areas including chemical engineering and biological science.[1–6] A thorough understanding of their structural and dynamic properties is essential for their applications. Debye and Hückel[7] proposed a homogeneous scenario, which only considers the two-point spatial correlation and is only applicable to extremely dilute aqueous ionic solutions whose concentration is less than 0.01 M. However, as the concentration increases, more ions interact with each other and one has to take higher order correlations into account.[7] A direct result of the correlation is multi-sized transient cluster formation and dissociation in aqueous ionic solutions, as already observed in some experiments and computer simulations. Georgalis *et al.*[8] observed experimentally cluster formation in NaCl and $(NH_4)_2SO_4$ solutions using dynamic light scattering. Cluster formation and its evolution in concentrated aqueous solutions of alkali thiocyanate salt have been experimentally observed by using 2D vibrational energy transfer.[9] Cluster formation in NaCl solution has been observed at ambient or supercritical conditions by different experimental groups.[10–13] Hassan[14,15] found the formation of variously sized clusters in NaCl solutions by molecular dynamics (MD) simulation and explored the structural and dynamic properties of ion clusters. Liquid-like polymer chains were identified by Wallace *et al.* in $CaCO_3$ solutions which act as the nuclei for crystallization.[16] Choi *et al.*[17–22] have adopted graph theory, MD simulations, density functional theory and experimental methods to systematically study cluster formation in different aqueous ionic solutions including NaCl, KSCN, $KClO_4$, *etc.* Our previous MD simulations[23] have demonstrated that, below the crystallization concentration, the spatial distribution of ions is homogeneous from the ensemble-averaged viewpoint but is instantly inhomogeneous. Since ions are distributed inhomogeneously in aqueous ionic solutions at a finite concentration due to transient cluster formation, it is interesting to see whether the dynamics of aqueous ionic solutions at room temperature are also heterogeneous, analogous to supercooled liquids?

Dynamic heterogeneity is a key feature of supercooled liquids, in which various relaxation processes simultaneously exist. The time correlation function usually decays in a stretched

[a] *Department of Physics, Civil Aviation Flight University of China, Guanghan, China*
[b] *State Key Laboratory of Environment-Friendly Energy Material, Southwest University of Science and Technology, Mianyang, China*
[c] *CAS Key Laboratory of Theoretical Physics, Institute of Theoretical Physics, Chinese Academy of Sciences, Beijing, China. E-mail: wangyt@itp.ac.cn*
[d] *School of Physical Sciences, University of Chinese Academy of Sciences, Beijing, China*

† Electronic supplementary information (ESI) available. See DOI: 10.1039/c8cp02787k

exponential manner at a long-time scale rather than the standard exponential decay in simple liquids.[24–27] Dynamic heterogeneity in glass-forming liquids has been systematically studied experimentally[28,29] and theoretically.[30–34] Keys *et al.*[28] detected the spatially heterogeneous dynamics in a system of air-driven granular beads by varying the density and effective temperature. They observed that the dynamics become much slower and more spatially heterogeneous when approaching the jamming transition point. Weeks *et al.*[29] have used confocal microscopy to directly observe the three-dimensional dynamics of colloidal supercooled glass and supercooled fluids. They found that mobile particles form clusters and show collective dynamics, and the average cluster size increases sharply near the glass transition point. Giovambattista *et al.*[30,35] studied the heterogeneous dynamics of supercooled water by performing molecular dynamics simulation with the SPC/E water model. They found that mobile water molecules form clusters, whose behaviour depends on the temperature. Moreover, ionic liquids perform as supercooled liquids even at room and higher temperatures with mobile ions strongly correlated[32] and cationic alkyl side chains diffusing collectively,[36] which should be correlated with their microscopic structural heterogeneity[35,37–40] and critical fluctuations.[41] Similar phenomena are also observed in supercooled Lennard-Jones liquids where mobile particles tend to form string-like clusters and diffuse together.[33,34]

Dynamic heterogeneity in aqueous ionic solutions at low temperatures in supercooled states was revealed in some dielectric and conductivity relaxation experiments, which however were more focused on water instead of aqueous ionic solutions. Experimental studies discovered that the response of aqueous ionic solutions presents more than one relaxation within a wide temperature range in a supercooled state, and the susceptibility can be fitted by the Cole–Cole equation[42–46] rather than the Debye exponential relaxation. As a good glass former, the fragility, decoupling, and glass transition of aqueous ionic solutions can be easily adjusted at low temperatures,[47] whose temperature dependence of the relaxation time obeys a super-Arrhenius law instead of the standard Arrhenius law.[48] A larger decoupling was observed in $Ca(NO_3)_2$ solutions compared to LiCl solutions.[48–50] Besides, aqueous ionic solutions can be more deeply supercooled than pure water, which facilitates their usage as a route to reach no man's land.[51,52] It was also shown that heat capacity and density anomalies are still present in dilute NaCl aqueous solutions but disappear at high concentrations.[53] Suzuki and Mishima[54] observed two distinct glassy states in diluted NaCl solutions. Polyamorphic phase separation caused by decompression was observed in LiCl aqueous solutions.[55,56] The glass-forming ability of LiCl solutions was studied by Kobayashi and Tanaka,[57,58] who found that the glass-forming ability is maximized near the eutectic point. Corradini *et al.*[59] found a liquid–liquid critical point in NaCl aqueous solutions at a higher temperature and lower pressure compared to pure water.

Since all the above studies for aqueous ionic solutions were conducted at low temperatures, it is still unclear whether aqueous ionic solutions at a finite concentration at room or even higher temperatures have heterogeneous dynamics. Some studies seem to hint at the existence of dynamic heterogeneity in ionic solutions at room temperature. Hassan[14] found variously sized clusters with different lifetimes in NaCl aqueous solutions. Zhang *et al.*[60] observed the deviation of dynamics from the Stokes–Einstein–Debye relation in KSCN aqueous solutions. Xiao and Song[61,62] have shown the electric potential around an ion has a multi-Yukawa form, and multi-Debye lengths exist in aqueous ionic solutions. However, so far no explicit and systematic studies focusing on this topic have been conducted. In this work, we carry out MD simulations for KSCN aqueous solutions as an example to explicitly identify the existence of dynamic heterogeneity in ionic solutions at a finite concentration at room and higher temperatures far above their glass transition temperature. To characterize the dynamic heterogeneity, we calculated the non-Gaussian parameters and self-van Hove functions for ions, both of which turned out to deviate from Gaussian in time and space. The ionic dynamic susceptibility is nonzero at intermediate times. The self-intermediate scattering functions for ions decay by following a stretched exponential function with an exponent β smaller than one, rather than the regular exponential decay in simple liquids. As ions tend to form transient clusters, we found that differently sized clusters relax by following stretched exponential functions with different times and exponents. The dynamics of ionic solutions are more homogeneous at a higher temperature. In addition, we propose that the relaxation of ionic solutions follows a mixed scenario instead of the pure homogeneous or inhomogeneous scenario. Variants of the Stokes–Einstein relation break down due to dynamic heterogeneity and a fractional form is followed, but the original Stokes–Einstein relation is actually fulfilled after taking into account the temperature dependence of the effective hydrodynamic radius.

2 Simulation details and analysis methods

2.1 Simulation details

Because of the high solubility of KSCN in water (24.49 mol kg^{-1} at $T = 298.15$ K),[63] KSCN aqueous solutions are a good choice to serve as a representative system for studying dynamic heterogeneity in ionic solutions since good statistics can be obtained with a moderate concentration corresponding to a not-too-large MD setup. The potassium ion parameters were adopted from the Dang model,[64,65] SCN^- parameters were taken from the model developed by Vincze *et al.*,[66] and water molecules were simulated by the SPC/E model.[41] All ions and atoms were treated as charged Lennard-Jones particles whose interactions are described as

$$u(r_{ij}) = 4\varepsilon_{ij}\left[\left(\frac{\sigma_{ij}}{r_{ij}}\right)^{12} - \left(\frac{\sigma_{ij}}{r_{ij}}\right)^{6}\right] + \frac{q_i q_j}{r_{ij}} \quad (1)$$

where r_{ij} is the distance between the ith atom (ion) and the jth atom (ion), σ and ε are the Lennard-Jones distance and energy

Table 1 Force field parameters for K^+, SCN^- and water molecules

Atom/ion	σ (nm)	ε (kJ mol^{-1})	Charge (e)
K^+	0.333	0.420	+1.0
S	0.352	1.5225	−0.56
C	0.335	0.425	+0.14
N	0.331	0.310	+0.58
O	0.3166	0.650	−0.8476
H	—	—	+0.4328

parameters, respectively, and q_i is the partial charge of the ith atom (ion). The corresponding force field parameters are listed in Table 1.

All our MD simulations were carried out with the GROMACS package,[67,68] and the system temperature was kept constant by the Nosé–Hoover thermostat.[69,70] Periodic boundary conditions were applied to all three dimensions and the particle mesh Ewald algorithm[71] was employed to calculate the long-range electrostatic interactions with a cutoff of 1.2 nm in real space. The van der Waals interactions were calculated directly with the same cutoff of 1.2 nm. The SCN^- and water molecules were kept rigid by constraining the bond lengths and angles at their equilibrium values by utilizing the SHAKE algorithm.[72] The Lorentz–Berthelot rule[73] was used to combine the Lennard-Jones potential parameters. We performed MD simulations for a KSCN aqueous solution with 300 ion pairs and 1024 water molecules corresponding to a concentration of 16.67 mol kg^{-1}, so that the system does not crystallize in the temperature range from 300 K to 800 K. To make sure that this concentration setup is reasonable for the given force field parameters, we have calculated the radial distribution functions (RDFs) of ions at various temperatures, which are plotted in Fig. 1. We can see from those RDFs that no crystallization happens at any simulated temperatures.

The system density was determined by a 5 ns *NPT* MD simulation at T = 300 K and P = 1 atm after a short-time equilibration from a manually constructed initial configuration. After that, the system went through an annealing procedure in the *NVT* ensemble from T = 2000 K down to 1500, 1000, 800, 700, 600, 500, 450, 400, 350, and 300 K for 1 ns at each temperature. A series of 30 ns *NVT* simulations were then carried out to equilibrate the system at eight temperatures of T = 300, 350, 400, 450, 500, 600, 700, and 800 K, whose initial configurations were taken from the annealing process at the given temperatures. To avoid possible disturbance of the thermostat, *NVE* simulations further followed at various temperatures. At each temperature, the system was equilibrated in the *NVE* ensemble for 10 ns, followed by a 500 ps *NVE* MD simulation to sample data. The time step for all MD simulations was 1 fs and the configurations were sampled every 10 steps for data analysis. Considering the fast system relaxation within 100 ps, the sampling simulation time of 500 ps and the sampling interval of 10 steps are appropriate. The simulation results obtained from the *NVE* simulations were compared with those from the *NVT* simulations and similar results were yielded.

2.2 Non-Gaussian parameter

If a system has dynamic heterogeneity, the thermal movements of particles deviate from the Gaussian distribution at intermediate time intervals, just as observed in supercooled liquids.[74] A non-Gaussian parameter was adopted to characterize the deviation of the system dynamics from the Gaussian behaviour, which is defined as

$$\alpha_2(t) = \frac{3\langle \vec{r}^4(t)\rangle}{5\langle \vec{r}^2(t)\rangle^2} - 1 \quad (2)$$

where $\vec{r}(t)$ is the ion position at time t, and the acute brackets represent the ensemble average. $\alpha_2(t)$ is zero if particle movements obey the Gaussian distribution, and non-zero otherwise. $\alpha_2(t)$ reaches its maximum at an intermediate time t^* in a dynamically heterogeneous system.

2.3 Self-van Hove function

The self-van Hove function was also adopted to further characterize the deviation of the system dynamics from the Gaussian behaviour as a function of both distance and time, which describes the distribution of a particle from its initial position and is defined by

$$G_s(r,t) = \frac{1}{N}\sum_{i=1}^{N}\left\langle \delta\left(\left|\vec{r}_i(t) - \vec{r}_i(0)\right| - r\right)\right\rangle \quad (3)$$

The first-order approximation of $G_s(r,t)$ takes the Gaussian form as

$$G_0(r,t) = \left[\frac{3}{2\pi\langle \vec{r}^2(t)\rangle}\right]^{3/2} \exp\left[-3r^2/2\langle \vec{r}^2(t)\rangle\right] \quad (4)$$

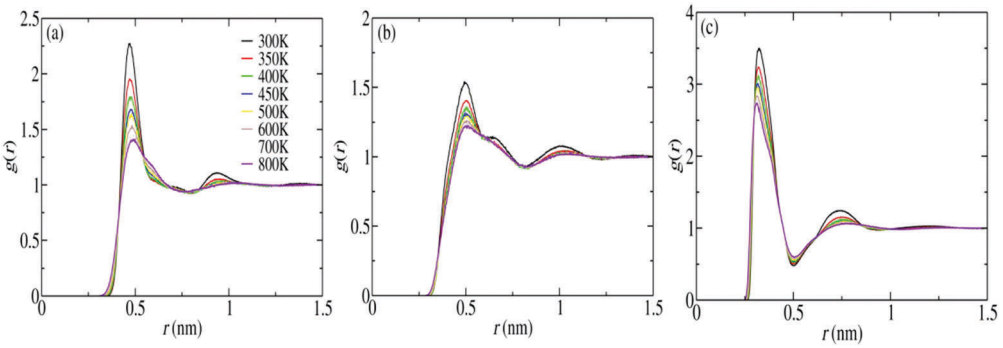

Fig. 1 Radial distribution functions of ions at various temperatures: (a) K^+–K^+, (b) SCN^-–SCN^-, and (c) K^+–SCN^-.

where $\langle \vec{r}^2(t) \rangle$ is the mean square displacement of ions. $G_s(r,t)$ deviates from $G_0(r,t)$ if the system dynamics is heterogeneous. We calculate the relative deviation $[G_s(r,t^*) - G_0(r,t^*)]/G_0(r,t^*)$ at time $t = t^*$, the most heterogeneous moment of $\alpha_2(t)$, to characterize the deviation from Gaussian in space.

2.4 Dynamical susceptibility

The dynamic susceptibility is usually applied to describe dynamic heterogeneity in supercooled liquids.[75] The maximum of the dynamic susceptibility characterizes the correlated volume and its appearance time corresponds to the correlation time. The dynamic susceptibility is defined as the fluctuation of the overlap function,[76] namely

$$\chi_4(t) = \frac{1}{N}[\langle Q^2(t) \rangle - \langle Q(t) \rangle^2] \quad (5)$$

where $Q(t)$ is the overlap function and is defined as[76,77]

$$Q(t) = \sum_{i=1}^{N} \delta\left(\left|\overrightarrow{r_i}(t_0) - \overrightarrow{r_i}(t_0 + t)\right|\right) \quad (6)$$

where $\delta(r) = 1$ if $r \leq r_{cut}$ and zero otherwise. The cutoff should be chosen in such a way that it is long enough to capture the correlation of particles while short enough to keep particles away from the influence of their images. In our case, the cutoff was chosen as the main peak position of the RDF between K^+ and SCN^-, which is $r_{cut} = 0.3$ nm. $\chi_4(t)$ is zero if the distribution of $Q(t)$ follows Gaussian behaviour, and nonzero otherwise.

2.5 Self-intermediate scattering function

To further identify the dynamic heterogeneity, we consider the structural relaxation of ions in aqueous ionic solutions. The relaxation of ions characterized by the self-intermediate scattering function is

$$F_s(k,t) = \frac{1}{N}\sum_{j}^{N} \left\langle \exp\left\{ i\overrightarrow{k} \cdot [\overrightarrow{r_j}(0) - \overrightarrow{r_j}(t)] \right\} \right\rangle \quad (7)$$

where N is the number of ions, and $k = |\vec{k}|$ is usually chosen as the position of the main peak of the static structure factor. In this wok, k values are 15.00 nm^{-1} for K^+ and 14.02 nm^{-1} for SCN^-, respectively. Detailed static structure factors are plotted in the ESI† (Fig. S1). Ions have a large fluctuation at $T = 300$ K, as shown by $S(0)$, and the fluctuation decreases significantly with increasing temperature. One charge order is formed at $k \sim 15$ nm^{-1} for both K^+ and SCN^-, and another is formed at $k \sim 15$ nm^{-1} and $k \sim 20$ nm^{-1} for K^+ and SCN^-, respectively.[64,78] $F_s(k,t)$ relaxes by following an exponential decay as $F_s(k,t) \sim e^{-t/\tau}$ in simple liquids, and a stretching exponential function $F_s(k,t) \sim e^{-(t/\tau)^\beta}$ in the α relaxation region in glass-forming liquids, where τ is the relaxation time and β is the exponent. β is usually smaller than 1 and its deviation from 1 also quantifies the degree of dynamic heterogeneity of the system.

2.6 Stokes–Einstein relation

The breakdown of the Stokes–Einstein relation is proposed to be a direct consequence of dynamic heterogeneity.[79] The Stokes–Einstein relation is expressed as

$$D = \frac{k_B T}{C\eta a} \quad (8)$$

where T is the temperature, k_B is the Boltzmann constant, η is the viscosity, a is the effective hydrodynamic radius of an ion, and C is a constant determined by boundary conditions. The ion diffusion constant is determined by its asymptotic relation with the mean square displacement

$$D = \lim_{t\to\infty} \frac{\left\langle \left|\overrightarrow{r_i}(t) - \overrightarrow{r_i}(0)\right|^2 \right\rangle}{6t} \quad (9)$$

Since η is difficult to accurately determine *via* simulation, τ is usually adopted as a substitute of η.[80] The two relations, $D \sim \tau^{-1}$ [81–83] and $D \sim T/\tau$,[84,85] are usually adopted as variants of the Stokes–Einstein relation. $D \sim \tau^{-1}$ is an exact result in simple liquids if the ion displacement $\delta\overrightarrow{r_j}(t) = \overrightarrow{r_j}(t) - \overrightarrow{r_j}(0)$ follows Gaussian behaviour. The same functional form is also proposed in the mode coupling theory if the temperature is close to the glass transition point.[79] $D \sim T/\tau$ comes from the approximated relation $\eta = G_\infty \tau$,[85] where G_∞ is the instantaneous shear modulus and presumed to be a constant.

Shi *et al.*[80] simulated three mixed Lennard-Jones-like liquids and coarse-grained *ortho*-terphenyl across a broad range of temperatures and densities, aiming to investigate the rationality of $D \sim \tau^{-1}$ and $D \sim T/\tau$ by comparing with the results given by $D \sim T/\eta$. They found that the two variants behave differently from $D \sim T/\eta$ during cooling. While the effective hydrodynamic radius a is often treated as a constant in $D \sim \tau^{-1}$, $D \sim T/\tau$ and $D \sim T/\eta$ when testing the Stokes–Einstein relation, in ionic solutions, a may vary with thermodynamic conditions due to the solvation effect and dielectric polarization.[65,86] Therefore, in the following, the Stokes–Einstein relation is evaluated by $D \sim T/\eta$ and $D \sim T/\eta a$, respectively, to study the influence of a.

2.7 Shear viscosity

Due to its reliability and fast convergence, the method proposed by Hess[87] has been adopted to calculate the shear viscosity. It is a non-equilibrium method with a periodic external force $a_x(z) = A\cos(qz)$ applied in the X direction, where A is the maximum of a_x and $q = 2\pi/l$ with l being the simulation box size. The Navier–Stokes equation for liquids with a_x applied is

$$\rho\frac{\partial u_x(z)}{\partial t} = \rho a_x(z) + \eta\frac{\partial^2 u_x(z)}{\partial z^2} \quad (10)$$

where the velocity $u_x(z)$ in the X direction is a function of z only and ρ is the density of the fluid. The consequent velocity for the steady state is

$$u_x(z) = V(1 - e^{-t/\tau})\cos(qz) \quad (11)$$

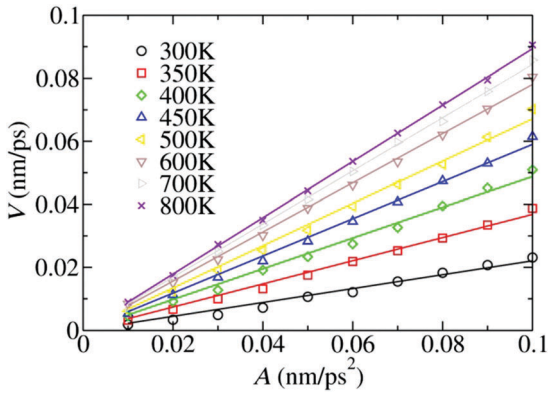

Fig. 2 The linear dependence regime between V and A at different temperatures. The symbols are simulation data and the solid lines are fitted by $V \sim A$.

where $V = A\rho/\eta q^2$ can be determined from $u_x(z)$. The shear viscosity is

$$\eta = \frac{A\rho}{Vq^2} \tag{12}$$

Because ρ and q are the same for all simulations, we evaluate the shear viscosity by A/V. The value of A needs to be chosen carefully to accurately determine the shear viscosity:[87] if A is too large, the system is too far from the equilibrium; if it is too small, the fluctuation is too large to accurately determine the viscosity. To obtain the correct shear viscosity, we determined the linear dependence regime between V and A and the temperature drift was kept smaller than 1 K. Fig. 2 shows that V is proportional to A when A is within 0.01–0.1 nm ps^{-2}.

2.8 Frictional coefficient

Because ions are charged in aqueous ionic solutions, we can calculate their frictional coefficient by applying an external static electric field E.[88,89] After reaching the non-equilibrium steady state, the frictional force on an ion ($f_r = \alpha v$) is equal to the electric force ($F_e = qE$), namely $qE = \alpha v$, where q is the electric charge of the ion, and v is the drift velocity dragged by E. The frictional coefficient is

$$\alpha = \frac{qE}{v} \tag{13}$$

where v can be calculated by $v = \lim_{t\to\infty} \langle r(t)\rangle/t$.[89] The frictional coefficient can be evaluated by $\alpha \sim E/v$ when q is a constant. The hydrodynamic radius of the ion is evaluated by $a \sim E/\eta v$. To prevent the system from moving too far from the equilibrium state, we determined the linear response region for K^+ and SCN^-, as shown in Fig. 3, in which v is proportional to E when E is within 0.01–0.1 V nm^{-1} for all temperatures.

3 Results and discussion

To identify the existence of dynamic heterogeneity in aqueous ionic solutions at room or even higher temperatures, we first characterize the thermal movements of ions in time and space

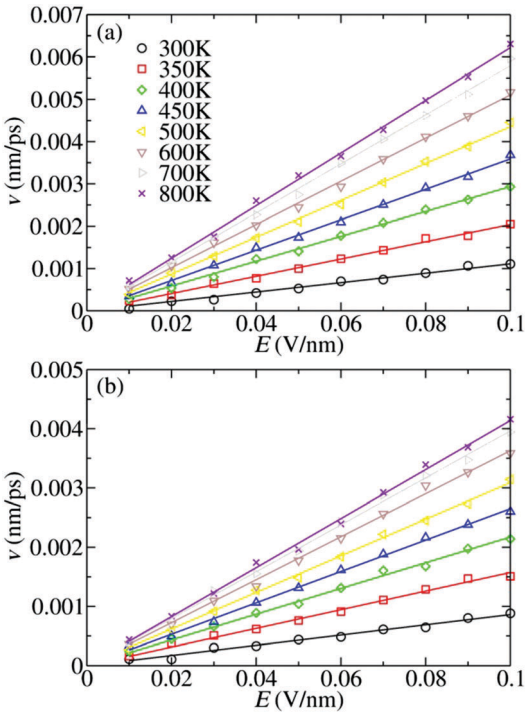

Fig. 3 The linear response region for K^+ and SCN^- under E at different temperatures. The symbols are simulation data and the solid lines are fitted by $v \sim E$.

by the non-Gaussian parameter and the self-van Hove function, respectively, followed by calculating the dynamic susceptibility of ions, and then calculate the structural relaxation. The microscopic mechanism of the dynamic heterogeneity was determined by calculating relaxation times of differently sized clusters, which manifests that dynamic heterogeneity in aqueous ionic solutions is attributed to ion cluster formation and dissociation. Finally, the Stokes–Einstein relation and its variants as well as their connections with dynamic heterogeneity are discussed.

3.1 Deviation from the Gaussian behavior

To identify if the system dynamics is heterogeneous, we first quantify the thermal movement of ions by calculating the non-Gaussian parameter α_2 and its change with time to see if it is Gaussian or not. The calculated α_2 for K^+ and SCN^- at temperatures 300, 350, and 400 K are plotted in Fig. 4, which shows similar changes as in glass-forming liquids:[34,79] α_2 is zero in the short-time range, followed by a gradual increase to reach its maximum value at $t = t^*$ in the intermediate time range, and then slowly decreases from its maximal value to its long-time limit of zero. The nonzero values of α_2 imply the deviations from Gaussian of ion displacements at intermediate times. The deviation from the Gaussian behaviour in aqueous ionic solutions is qualitatively the same as in supercooled liquids.[34,90,91] Both the maximal values of α_2 and t^* decrease with increasing temperature, demonstrating that the dynamics of the KSCN solution becomes more homogeneous at a higher temperature. The maximal values of α_2 at different temperatures are smaller than those observed in supercooled Lennard-Jones liquids,[34]

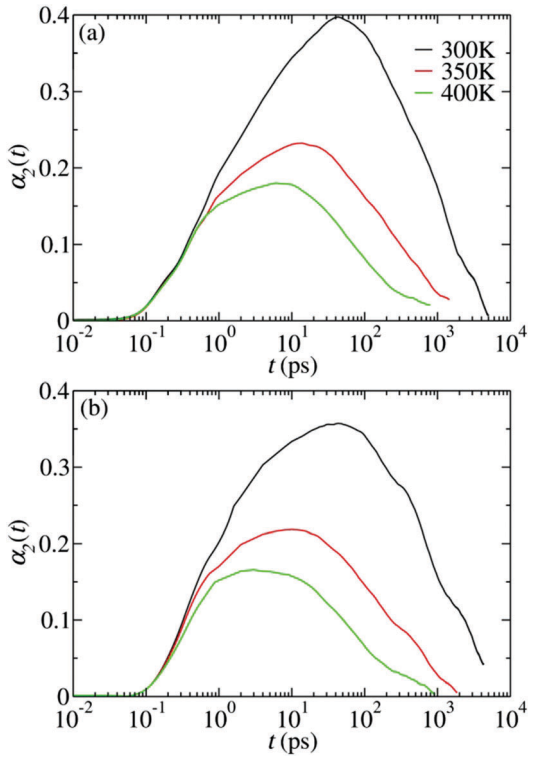

Fig. 4 Non-Gaussian parameter α_2 *versus* time t at temperatures 300, 350, and 400 K for K^+ (a) and SCN^- (b).

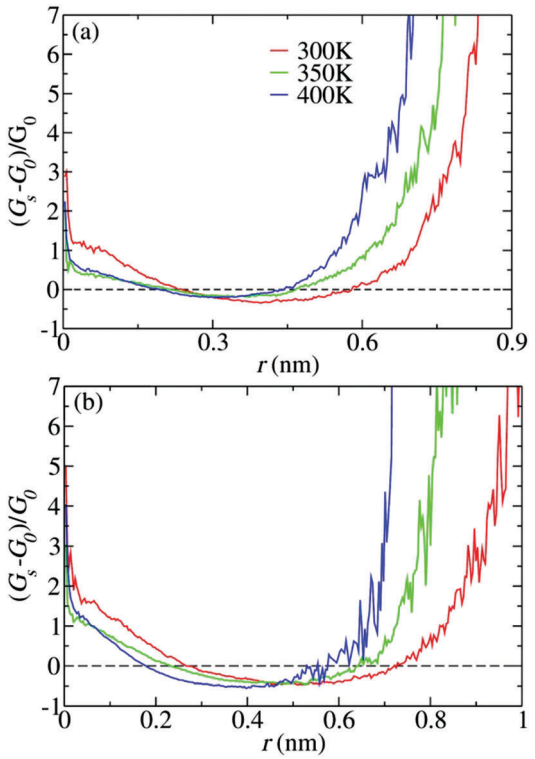

Fig. 5 $[G_s(r,t^*) - G_0(r,t^*)]/G_0(r,t^*)$ *versus* r at time $t = t^*$ and temperatures T = 300, 350, and 400 K for K^+ (a) and SCN^- (b).

indicating that dynamic heterogeneity in ionic solutions at room and higher temperatures is relatively weak.

To further quantify the dynamic heterogeneity, we calculate the self-van Hove functions $G_s(r,t)$ for K^+ and SCN^- at time $t = t^*$, which are compared with their first-order approximations. All the relative deviations $[G_s(r,t^*) - G_0(r,t^*)]/G_0(r,t^*)$ at time $t = t^*$ plotted in Fig. 5 show the same trend: the deviations are around four at the initial point $r = 0$, and start to decrease with distance; after decreasing to its first zero, the deviation continues decreasing to be negative; after reaching the minimal negative value, it starts increasing which becomes significant beyond r^*. Moreover, similar to α_2, the deviation significantly decreases with increasing temperature. Those results are similar to those for supercooled Lennard-Jones liquids.[34]

The dynamic susceptibility $\chi_4(t)$[76] is adopted to further characterize the dynamic heterogeneity. $\chi_4(t)$ of K^+ and SCN^- at T = 300, 350 and 400 K are plotted in Fig. 6. Similar as in supercooled liquids,[76] each $\chi_4(t)$ is almost zero at short times, reaches its maximum at intermediate times, and decreases to zero at long times, suggesting that the distribution of $Q(t)$ deviates from Gaussian. The correlation volume decreases with increasing temperature as well as the correlation time, and the dynamic heterogeneity also decreases with increasing temperature. The maximum of $\chi_4(t)$ is much smaller than that observed in supercooled Lennard-Jones liquids,[74,75] and the dynamic heterogeneity is much smaller in aqueous ionic solutions compared with supercooled liquids at a much lower temperature. Overall, combining the results given by

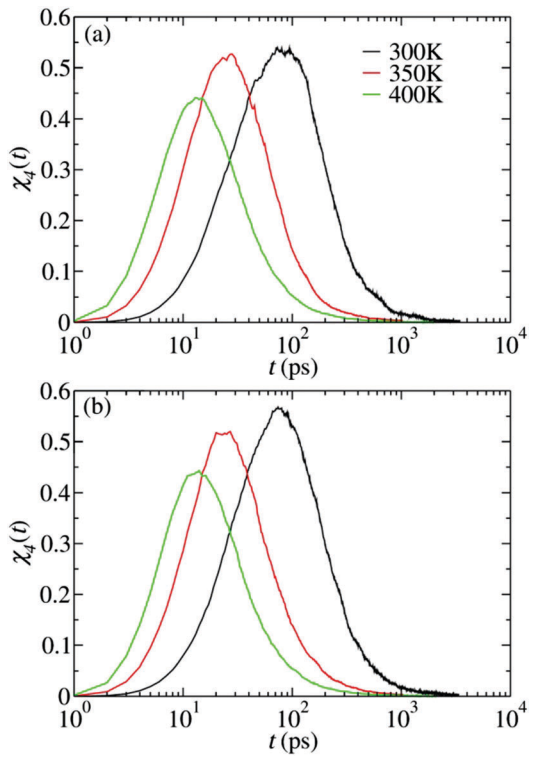

Fig. 6 Dynamic susceptibility $\chi_4(t)$ as a function of time t at temperatures T = 300, 350, and 400 K for K^+ (a) and SCN^- (b).

the non-Gaussian parameter, self-van Hove function and dynamic susceptibility, it is verified that the dynamics of aqueous ionic solutions are unambiguously heterogeneous at room and even higher temperatures, which become more homogeneous at a higher temperature. Nevertheless, the dynamic heterogeneity in ionic solutions at room temperature is weaker than that in supercooled liquids at a much lower temperature.

3.2 Structural relaxation

In systems with dynamic heterogeneity, the time correlation function decays in a stretched exponential way at large times rather than the standard exponential relaxation in simple liquids.[92] The calculated self-intermediate scattering functions $F_s(k,t)$ for K^+ and SCN^- are shown in Fig. 7. It is shown that $F_s(k,t)$ decays much faster than in glass-forming liquids,[34,81,93] and a higher temperature leads to a faster decay. Besides, no obvious plateaus indicating β relaxation, typical in glass-forming and supercooled liquids at low temperatures, have been observed in our simulations, which can be understood by the fact that, in aqueous ionic solutions at room or even higher temperatures, ions have more freedom to move without being fully arrested in local cage structures.

To test if ions relax exponentially, $F_s(k,t)$ have been fitted by $F_s(k,t) \sim e^{-(t/\tau)^\beta}$ and the fitted βs are plotted in Fig. 8. All βs are smaller than 1, demonstrating that $F_s(k,t)$ follows a stretched exponential decay at long times rather than the standard exponential decay. The β value increases and approaches 1 with increasing temperature, indicating that the system dynamics are more homogeneous at a higher temperature, consistent with the results from the non-Gaussian parameter, self-van Hove function and dynamic susceptibility.

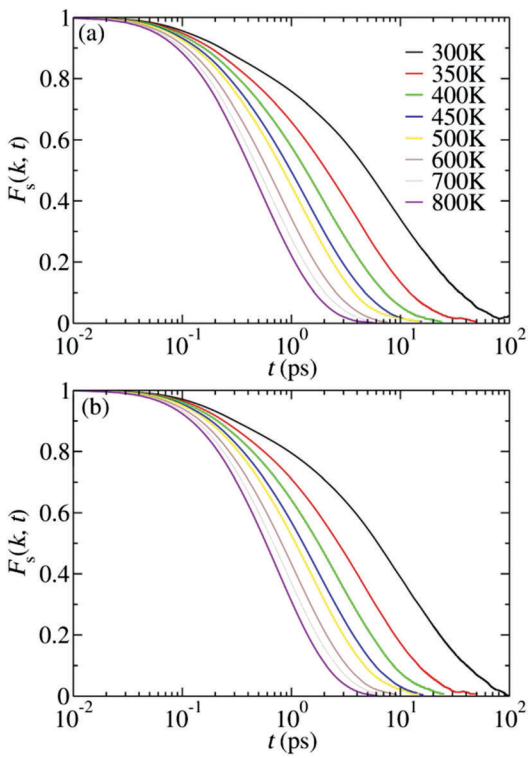

Fig. 7 Self-intermediate scattering functions $F_s(k,t)$ at different temperatures for K^+ (a) and SCN^- (b).

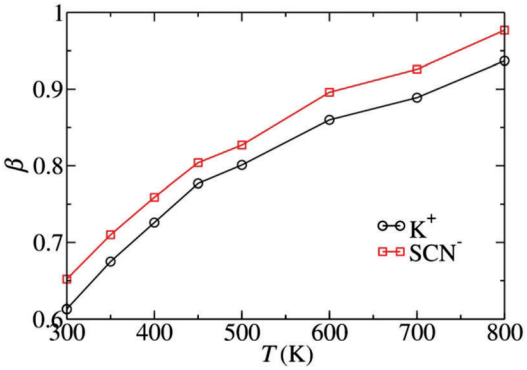

Fig. 8 Exponents β for the self-intermediate scattering functions fitted by $F_s(k,t) \sim e^{-(t/\tau)^\beta}$.

3.3 Relaxation scenario

All the above results indicate that aqueous ionic solutions have similar dynamic heterogeneity with supercooled liquids. In this section, we investigate the relaxation scenario of ionic solutions. Two extreme macroscopic scenarios[30,79] have been proposed to explain the non-exponential relaxation in glass-forming liquids: in the homogeneous scenario, the time correlation functions for different components decay by following the same stretched exponential function; in the heterogeneous scenario, different components decay by following the standard exponential function but with different relaxation times, and the superposition of all components results in a stretched exponential function.

To study the relaxation scenario in ionic solutions, we quantify the size distributions of ion clusters by adopting the definition of a cluster proposed by Stillinger[94] that a particle belongs to a cluster if the distance between this particle and one of the particles in this cluster is smaller than a certain distance r_{cut}. In this work, r_{cut} is chosen as the position of the main peak of $g_{K-K}(r)$ (0.45 nm) for K^+ and $g_{SCN-SCN}(r)$ (0.5 nm) for SCN^-. The size distributions for clusters consisting of K^+ or SCN^- are shown in the ESI,† (Fig. S2, Tables S1 and S2). Most clusters are smaller than 7 and larger size clusters have smaller probabilities to appear. The lifetimes of clusters[14] with size 2–7 have also been calculated and are plotted in the ESI,† (Fig. S3). The clusters consisting of K^+ are less stable with increasing size and temperature, while a complex change is shown for SCN^-.

Since the majority of ions belong to clusters with sizes between 1 and 7, the self-van Hove functions for clusters with various sizes from 1 to 7 for K^+ and SCN^- have been calculated and fitted by $F_s(k,t) \sim e^{-(t/\tau)^\beta}$ to obtain τ and β, as plotted in Fig. 9, and the mean values and their fluctuation of different clusters are plotted in Fig. 10. It can be seen that clusters with different sizes decay with different lifetimes τ and exponents β, both of which fluctuate heavily at low temperatures. With increasing temperature, the fluctuations are suppressed with decreasing τ and increasing β which approaches one. All clusters

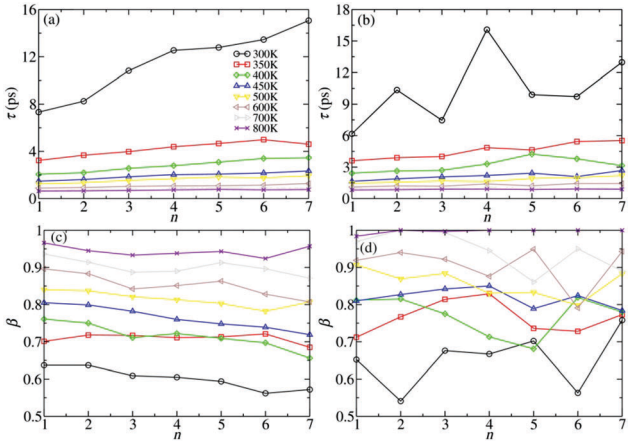

Fig. 9 τ and β of the self-van Hove functions for differently sized clusters fitted by $F_s(k,t) \sim e^{-(t/\tau)^{\beta}}$ at different temperatures: (a) and (b) for K^+; (c) and (d) for SCN^-.

relax faster with increasing temperature and correspondingly the dynamics become more homogeneous. Those results manifest that various relaxation processes simultaneously exist in ionic solutions and differently sized clusters relax with different τ and β. The lifetimes τ and exponents β of clusters are not equal, as shown in Fig. 9, demonstrating that ionic solutions follow a mixture of the pure homogeneous scenario and the pure heterogeneous scenario.

It has been shown that cluster formation plays an important role in the relaxation scenario in ionic solutions: ions are likely

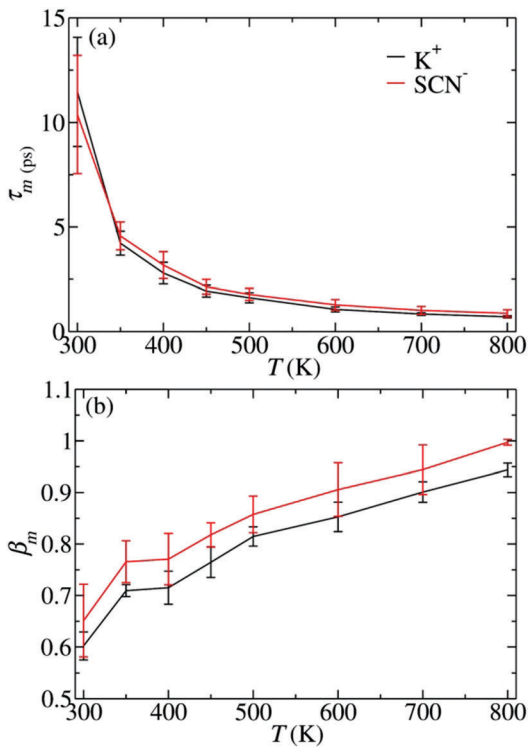

Fig. 10 The mean values of τ and β for different sized clusters. The error bars demonstrate the fluctuations of τ_m and β_m.

to form more diverse and larger sized clusters in concentrated solutions.[15,23] To further examine the role of cluster formation in ionic solutions, we also calculated the dynamic heterogeneity in different concentrations at T = 300 K. The dynamic heterogeneity with decreasing concentration shows similar changes to when the temperature increases. The dynamic susceptibility, fitted β for K^+ and SCN^-, fitted τ and β for clusters with size 1–7 and cluster distributions are listed in the ESI,† (Fig. S3–S6, Tables S3 and S4). Ions form smaller clusters at a lower concentration, and large clusters rarely appear. Moreover, the ionic solution is dynamically more homogeneous at a lower temperature. Differently sized clusters relax with different τ and β, and more diverse τ and β are observed at a larger concentration. The results also indicate that ionic solutions relax in a mixed scenario, and cluster formation plays an important role in the relaxation of ionic solutions.

3.4 Stokes–Einstein relation and its variants

The two variants of the Stokes–Einstein relation, $D \sim \tau^{-1}$ [81–83] and $D \sim T/\tau$,[84,85] are usually adopted to evaluate the Stokes–Einstein relation in supercooled liquids. The breakdown of the Stokes–Einstein relation is proposed to be a direct consequence of dynamic heterogeneity.[79] Shi *et al.*[80] have found that the usually adopted two variants of the Stokes–Einstein relation, $D \sim \tau^{-1}$ and $D \sim T/\tau$, give different results from $D \sim T/\eta$ in supercooled Lennard-Jones-like liquids and coarse-gained *ortho*-terphenyl when the temperature decreases, so they have concluded that $\eta \sim T\tau$ and $\eta \sim \tau$ are not good in evaluation of η. On the other hand, a may not be a constant in ionic solutions, so we take into account a to test the Stokes–Einstein relation with $D \sim \tau^{-1}$, $D \sim T/\tau$, $D \sim T/\eta$ and $D \sim T/\eta a$, respectively, to identify whether the dynamic heterogeneity indeed leads to the breakdown of the Stokes–Einstein relation in aqueous ionic solutions.

The diffusion constants and structural relaxation times at different temperatures are plotted in Fig. 11. $D \sim \tau^{-1}$ and $D \sim T/\tau$ are evaluated by $D \sim \tau^{-\xi_1}$ and $D \sim (T/\tau)^{\xi_2}$, respectively. Fig. 12(a) shows that the calculated D and τ are well fitted by $D \sim \tau^{-\xi_1}$ with $\xi_1 = 1.17$ for K^+ and 1.12 for SCN^-, demonstrating that $D \sim \tau^{-1}$ breaks down and follows a fractional form.[81] Due to different temperature dependences of D and τ, $\xi_1 < 1$ in ionic liquids[81] but $\xi_1 > 1$ in this work: the increase of D is faster than the decrease of τ in aqueous ionic solutions while heating, but a reverse trend is observed in ionic liquids. As shown in Fig. 12(b), the data can also be well fitted by $D \sim (T/\tau)^{\xi_2}$ with $\xi_2 = 0.74$ for K^+ and 0.70 for SCN^-, indicating that $D \sim T/\tau$ is also invalid, and ξ_2 is smaller than 1 analogous to that observed in supercooled water.[84,85]

Inside the linear dependence regime shown in Fig. 3, the shear viscosity evaluated by $\eta \sim A/V$ is calculated and plotted in Fig. 13(a), which decreases with increasing temperature. All the data shown in Fig. 13(b) align along the line described by $D \sim (T/\eta)^{\xi_3}$ with $\xi_3 = 1.13$ for K^+ and 1.04 for SCN^-. The deviation of ξ_3 from 1 indicates that the Stokes–Einstein relation described by $D \sim T/\eta$ is also invalid. In the cases of $D \sim \tau^{-1}$ and $D \sim T/\tau$, the shear viscosity is evaluated

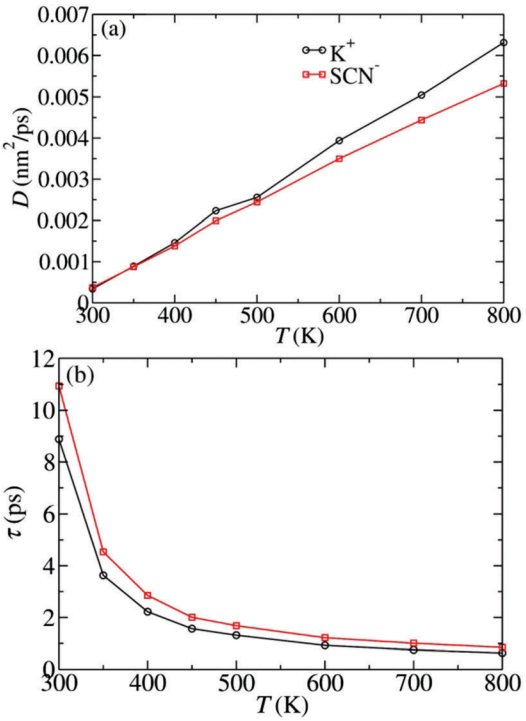

Fig. 11 The diffusion constant D (a) and the structural relaxation time τ (b) for K^+ and SCN^- at different temperatures.

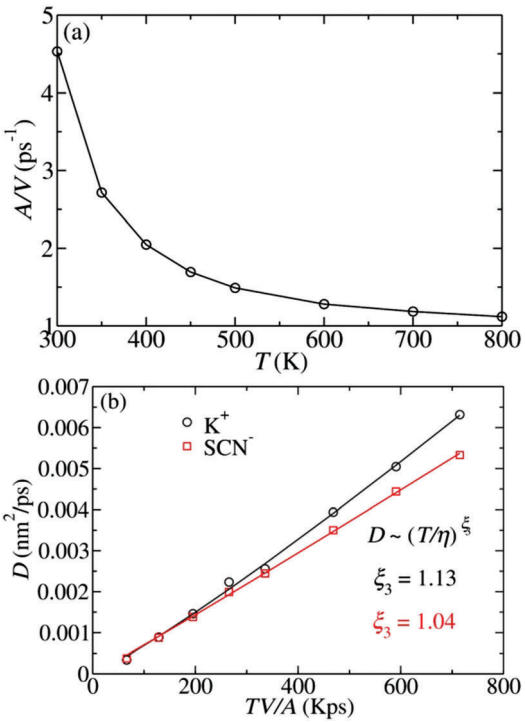

Fig. 13 (a) Shear viscosity evaluated by $\eta \sim A/V$. (b) Testing the Stokes–Einstein relation with $D \sim T/\eta$. The symbols are the simulated results and the solid lines are fitted by $D \sim (T/\eta)^{\xi_3}$.

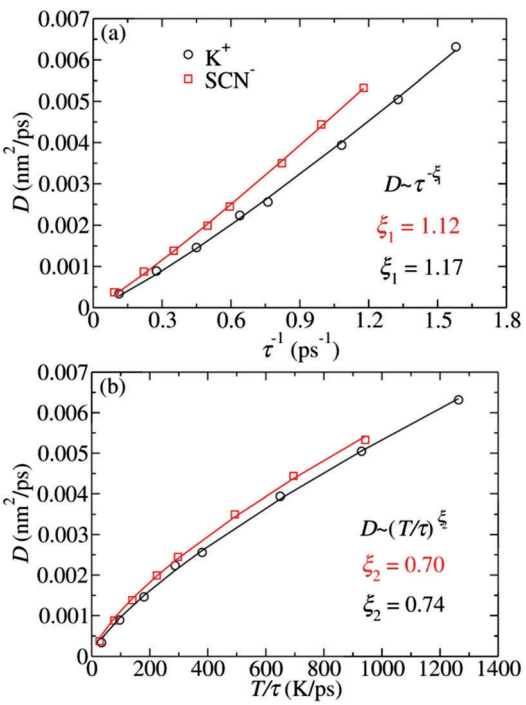

Fig. 12 Testing the Stokes–Einstein relation with its two variants, $D \sim \tau^{-1}$ and $D \sim T/\tau$. The symbols are the simulated results and the solid lines are fitting by $D \sim \tau^{-\xi_1}$ and $D \sim (T/\tau)^{\xi_2}$, respectively. The fitted exponent ξ_1 or ξ_2 is in the same colour as the fitted solid line.

by $\eta \sim T\tau$ and $\eta \sim \tau$, respectively. All ξs are different in $D \sim \tau^{-\xi_1}$, $D \sim (T/\tau)^{\xi_2}$ and $D \sim (T/\eta)^{\xi_3}$ for both K^+ and SCN^-, indicating that the forms of $\eta \sim T\tau$ and $\eta \sim \tau$ are invalid. The deviations of $D \sim (T/\eta)^{\xi_3}$ from 1 are smaller than $D \sim \tau^{-\xi_1}$ and $D \sim (T/\tau)^{\xi_2}$, demonstrating that $D \sim T/\eta$ is better than $D \sim \tau^{-1}$ and $D \sim T/\tau$ in verifying the Stokes–Einstein relation. ξ_1 for $D \sim \tau^{-\xi_1}$ is close to ξ_3 given by $D \sim (T/\eta)^{\xi_3}$, suggesting that $\eta \sim T\tau$ may be a better substitute than $\eta \sim \tau$ for aqueous ionic solutions, as similarly observed by Shi *et al.*[80]

To verify whether the original Stokes–Einstein relation $D \sim T/\eta a$ is really invalid or not, we should take into account the temperature dependence of the effective hydrodynamic radius and consider the frictional coefficient $\alpha \sim \eta a$. The frictional coefficient evaluated by $\alpha \sim E/v$ with data is shown in Fig. 3. Fig. 14(a) shows that the frictional coefficients decrease with increasing temperature; and Fig. 14(b) shows that the simulation data can be well fitted by $D \sim (T/\alpha)^{\xi_4}$ with ξ_4 almost equal to 1 for both K^+ and SCN^-. The results suggest that the Stokes–Einstein relation $D \sim T/\eta a$ is actually valid in ionic solutions at room and higher temperatures even with dynamic heterogeneity.

Because of the dynamic heterogeneity, the displacement of the ion deviated from Gaussian and further leads to the breakdown of $D \sim \tau^{-1}$. The variant $D \sim T/\tau$ is based on the approximated relation $\eta = G_\infty \tau$ and G_∞ is presumed to be independent of temperature. However, the different ξ for $D \sim (T/\tau)^{\xi_2}$ and $D \sim (T/\eta)^{\xi_3}$ indicate that $\eta = G_\infty \tau$ is invalid in our simulations, and the temperature dependence of G_∞ is also observed in Lennard-Jones-like liquids and coarse-grained ortho-terphenyl.[80] Therefore, care should be taken when $\eta \sim T\tau$ and

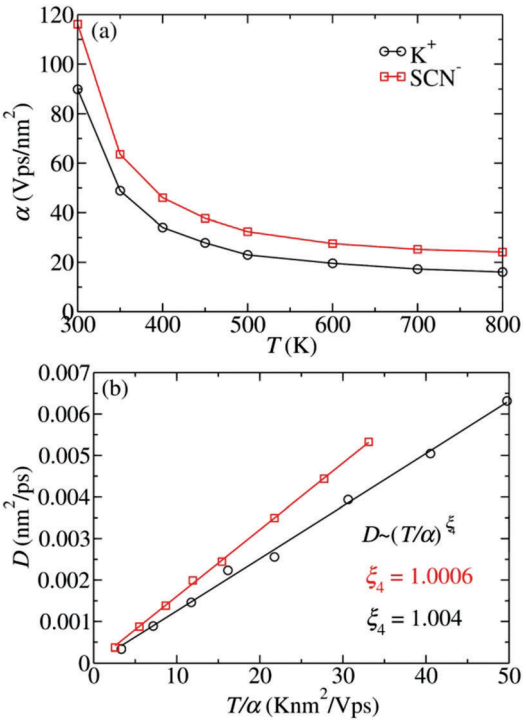

Fig. 14 (a) The frictional coefficient evaluated by $\alpha \sim E/v$. (b) Testing the Stokes–Einstein relation with $D \sim T/\alpha$. The symbols are the simulated results and the solid lines are fitted by $D \sim (T/\alpha)^{\xi_4}$.

$\eta \sim \tau$ are used to test the validity of the Stokes–Einstein relation. The effective hydrodynamic radius has been evaluated by $a \sim \alpha/\eta$, and the scaled effective hydrodynamic radius $\bar{a}$ is plotted in Fig. 15. $\bar{a}$ is not a constant, but almost decreases with increasing temperature for K^+ and SCN^-, indicating that the effective hydrodynamic radius is not always a constant, especially when thermodynamic conditions change significantly. By comparing the results given by $D \sim \tau^{-1}$, $D \sim T/\tau$, and $D \sim T/\eta$ with $D \sim T/\eta a$, it is shown that the Stokes–Einstein relation $D \sim T/\eta a$ is actually valid above room temperature, despite the fact that the dynamic heterogeneity and the fractional form of the variants are observed. The results suggest that $D \sim \tau^{-1}$, $D \sim T/\tau$ and $D \sim T/\eta$ may not always be used as substitutes of the Stokes–Einstein relation $D \sim T/\eta a$. Moreover, the dynamic heterogeneity may not necessarily result in the breakdown of the Stokes–Einstein relation.

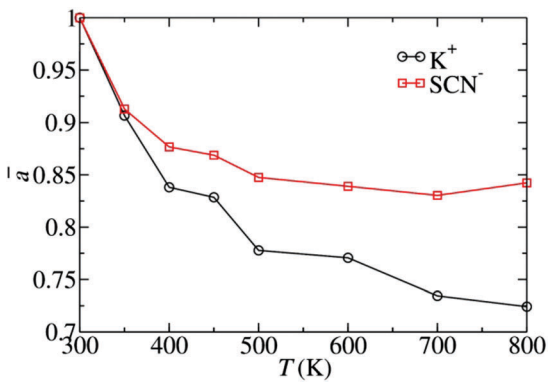

Fig. 15 The scaled effective hydrodynamic radius $\bar{a}$ for K^+ and SCN^- at different temperatures.

4 Conclusions

In this work, KSCN aqueous solutions were simulated by MD simulation as an example to probe the existence of dynamic heterogeneity in aqueous ionic solutions at room and higher temperatures. Our results indicate that dynamic heterogeneity does exist in ionic solutions at room and higher temperatures, analogous to supercooled liquids at much lower temperatures. The thermal movements of K^+ and SCN^- deviate from the Gaussian behaviour. The self-van Hove functions deviate from their first approximation and the deviation increases significantly at large distances. The dynamic susceptibility of ions is nonzero at intermediate time which also suggests deviations from Gaussian. The self-intermediate scattering functions of K^+ and SCN^- decay in a stretched exponential way. The solutions become dynamically more homogeneous at a higher temperature. Both the fluctuations of τ and β decrease with increasing temperature. Differently sized clusters relax with different τ and β, indicating that ionic solutions relax by following a mixture of the homogeneous and heterogeneous scenarios. In experiment, the simplest way to detect dynamic heterogeneity in ionic solutions is measuring the susceptibility of ionic solutions under an external applied electric field:[42–46] the dynamic heterogeneity is present if the susceptibility is in a non-Debye form. On the other hand, it is difficult and challenging to confirm the dynamic heterogeneity by directly measuring the relaxation or testing $D \sim \tau^{-1}$. A promising method is combining the work of Zhuang *et al.*[9,60] and Xu *et al.*[84] with the former directly measuring cluster formation by energy transfer and the latter directly detecting the relaxation.

The Stokes–Einstein relation is examined with the two commonly adopted variants, $D \sim \tau^{-1}$ and $D \sim T/\tau$. Our results show that both take fractional forms with $\xi \neq 1$ for K^+ and SCN^-. By comparing the results with $D \sim T/\eta$, it is suggested that $D \sim \tau^{-1}$ and $D \sim T/\tau$ are not good variants of the Stokes–Einstein relation described by $D \sim T/\eta$. The effective hydrodynamic radius is treated as a constant in $D \sim \tau^{-1}$, $D \sim T/\tau$, and $D \sim T/\eta$, while we have found that the effective hydrodynamic radius is not a constant but decreases with increasing temperature. After taking into account the effective hydrodynamic radius, it is shown that the Stokes–Einstein relation described by $D \sim T/\eta a$ is actually valid. Overall, the effective hydrodynamic radius may vary with thermodynamic conditions, so care should be taken when the three forms $D \sim \tau^{-1}$, $D \sim T/\tau$, and $D \sim T/\eta$ are used to test the Stokes–Einstein relation. Moreover, the dynamic heterogeneity may not result in the breakdown of the Stokes–Einstein relation.

The physical picture provided by our MD simulation results is that, at room temperature or even a higher temperature, the dynamic heterogeneity in ionic solutions is analogous to but a little weaker than that in glass-forming liquids at a much lower

temperature, and the structural heterogeneity caused by transient cluster formation results in the dynamic heterogeneity in ionic solutions.

Conflicts of interest

There are no conflicts to declare.

Acknowledgements

This work was supported by the National Natural Science Foundation of China (No. 21601164, 11774357, and 11747601). Y. W. also thanks the financial support through the CAS Biophysics Interdisciplinary Innovation Team Project (No. 2060299). The computations of this work were conducted on the HPC cluster of ITP-CAS.

References

1 J.-F. Equey, S. Müller, A. Tsukada and O. Haas, *J. Appl. Electrochem.*, 1989, **19**, 65–68.
2 B. Conway, *Chem. Soc. Rev.*, 1992, **21**, 253–261.
3 R. N. Zare, *Science*, 1988, **242**, 224–228.
4 J. A. White, *J. Chem. Phys.*, 1999, **111**, 9352–9356.
5 M. C. Gurau, S.-M. Lim, E. T. Castellana, F. Albertorio, S. Kataoka and P. S. Cremer, *J. Am. Chem. Soc.*, 2004, **126**, 10522–10523.
6 B. Roux and M. Karplus, *Annu. Rev. Biophys. Biomol. Struct.*, 1994, **23**, 731–761.
7 L. M. Varela, M. García and V. c. Mosquera, *Phys. Rep.*, 2003, **382**, 1–111.
8 Y. Georgalis, A. M. Kierzek and W. Saenger, *J. Phys. Chem. B*, 2000, **104**, 3405–3406.
9 H. Bian, X. Wen, J. Li, H. Chen, S. Han, X. Sun, J. Song, W. Zhuang and J. Zheng, *Proc. Natl. Acad. Sci. U. S. A.*, 2011, **108**, 4737–4742.
10 A. A. Chialvo and J. M. Simonson, *J. Mol. Liq.*, 2007, **134**, 15–22.
11 A. Chialvo, P. Cummings, H. Cochran, J. Simonson and R. Mesmer, *J. Chem. Phys.*, 1995, **103**, 9379–9387.
12 C. J. Fennell, A. Bizjak, V. Vlachy and K. A. Dill, *J. Phys. Chem. B*, 2009, **113**, 6782–6791.
13 L. Degrève and F. L. B. da Silva, *J. Chem. Phys.*, 1999, **111**, 5150.
14 S. A. Hassan, *J. Phys. Chem. B*, 2008, **112**, 10573–10584.
15 S. A. Hassan, *Phys. Rev. E: Stat., Nonlinear, Soft Matter Phys.*, 2008, **77**, 031501.
16 A. F. Wallace, L. O. Hedges, A. Fernandez-Martinez, P. Raiteri, J. D. Gale, G. A. Waychunas, S. Whitelam, J. F. Banfield and J. J. D. Yoreo, *Science*, 2013, **341**, 885–889.
17 J.-H. Choi and M. Cho, *J. Chem. Phys.*, 2016, **145**, 174501.
18 J.-H. Choi and M. Cho, *J. Chem. Phys.*, 2014, **141**, 154502.
19 J.-H. Choi and M. Cho, *J. Chem. Phys.*, 2016, **144**, 204126.
20 J.-H. Choi and M. Cho, *J. Chem. Phys.*, 2015, **143**, 104110.
21 J.-H. Choi, H. Kim, S. Kim, S. Lim, B. Chon and M. Cho, *J. Chem. Phys.*, 2015, **142**, 204102.
22 S. Kim, H. Kim, J.-H. Choi and M. Cho, *J. Chem. Phys.*, 2014, **141**, 124510.
23 R. Gan and W. Yanting, *EPL*, 2014, **107**, 30005.
24 J. P. Perdew and A. Zunger, *Phys. Rev. B: Condens. Matter Mater. Phys.*, 1981, **23**, 5048–5079.
25 C. Iuga, C. Solís, J. R. Alvarez-Idaboy, M. Á. Martínez, M. A. Mondragón and A. Vivier-Bunge, *J. Mol. Model.*, 2014, **20**, 2186.
26 A. D. Becke, *Phys. Rev. A: At., Mol., Opt. Phys.*, 1988, **38**, 3098–3100.
27 J. P. Perdew and Y. Wang, *Phys. Rev. B: Condens. Matter Mater. Phys.*, 1992, **45**, 13244–13249.
28 A. S. Keys, A. R. Abate, S. C. Glotzer and D. J. Durian, *Nat. Phys.*, 2007, **3**, 260–264.
29 K. Laasonen, R. Car, C. Lee and D. Vanderbilt, *Phys. Rev. B: Condens. Matter Mater. Phys.*, 1991, **43**, 6796–6799.
30 N. Giovambattista, M. G. Mazza, S. V. Buldyrev, F. W. Starr and H. E. Stanley, *J. Phys. Chem. B*, 2004, **108**, 6655–6662.
31 D. Jeong, M. Choi, H. J. Kim and Y. Jung, *Phys. Chem. Chem. Phys.*, 2010, **12**, 2001–2010.
32 M. G. Del Pópolo and G. A. Voth, *J. Phys. Chem. B*, 2004, **108**, 1744–1752.
33 C. Donati, J. F. Douglas, W. Kob, S. J. Plimpton, P. H. Poole and S. C. Glotzer, *Phys. Rev. Lett.*, 1998, **80**, 2338–2341.
34 W. Kob, C. Donati, S. J. Plimpton, P. H. Poole and S. C. Glotzer, *Phys. Rev. Lett.*, 1997, **79**, 2827.
35 R. Hayes, S. Imberti, G. G. Warr and R. Atkin, *Phys. Chem. Chem. Phys.*, 2011, **13**, 3237–3247.
36 Y. Wang and G. A. Voth, *J. Phys. Chem. B*, 2006, **110**, 18601–18608.
37 J. N. A. Canongia Lopes and A. A. H. Pádua, *J. Phys. Chem. B*, 2006, **110**, 3330–3335.
38 Y. Wang and G. A. Voth, *J. Am. Chem. Soc.*, 2005, **127**, 12192–12193.
39 A. Triolo, O. Russina, H.-J. Bleif and E. D. Cola, *J. Phys. Chem. B*, 2007, **111**, 4641–4644.
40 W. Schroer, A. Triolo and O. Russina, *J. Phys. Chem. B*, 2016, **120**, 2638–2643.
41 W. Schroer, S. Wiegand and H. Weingartner, *Berichte der Bunsengesellschaft für physikalische Chemie*, 1993, **97**, 975–981.
42 J. Barthel, R. Buchner, P. N. Eberspächer, M. Münsterer, J. Stauber and B. Wurm, *J. Mol. Liq.*, 1998, **78**, 83–109.
43 R. Buchner, G. T. Hefter and P. M. May, *J. Phys. Chem. A*, 1999, **103**, 1–9.
44 J. Ambrus, C. Moynihan and P. Macedo, *J. Phys. Chem.*, 1972, **76**, 3287–3295.
45 W. Wachter, W. Kunz, R. Buchner and G. Hefter, *J. Phys. Chem. A*, 2005, **109**, 8675–8683.
46 T. Chen, G. Hefter and R. Buchner, *J. Phys. Chem. A*, 2003, **107**, 4025–4031.
47 C. A. Angell, *Chem. Rev.*, 2002, **102**, 2627–2650.
48 C. T. Moynihan, N. Balitactac, L. Boone and T. A. Litovitz, *J. Chem. Phys.*, 1971, **55**, 3013–3019.
49 J. Ambrus, C. Moynihan and P. Macedo, *J. Electrochem. Soc.*, 1972, **119**, 192–198.
50 J. H. Ambrus, H. Dardy and C. T. Moynihan, *J. Phys. Chem.*, 1972, **76**, 3495–3501.

51 H. Kanno and C. Angell, *J. Phys. Chem.*, 1977, **81**, 2639–2643.
52 K. Miyata, H. Kanno, T. Niino and K. Tomizawa, *Chem. Phys. Lett.*, 2002, **354**, 51–55.
53 D. G. Archer and R. W. Carter, *J. Phys. Chem. B*, 2000, **104**, 8563–8584.
54 Y. Suzuki and O. Mishima, *Phys. Rev. Lett.*, 2000, **85**, 1322–1325.
55 O. Mishima, *J. Chem. Phys.*, 2005, **123**, 154506.
56 O. Mishima, *J. Chem. Phys.*, 2007, **126**, 244507.
57 M. Kobayashi and H. Tanaka, *J. Phys. Chem. B*, 2011, **115**, 14077–14090.
58 M. Kobayashi and H. Tanaka, *Phys. Rev. Lett.*, 2011, **106**, 125703.
59 D. Corradini and P. Gallo, *J. Phys. Chem. B*, 2011, **115**, 14161–14166.
60 Q. Zhang, W. Xie, H. Bian, Y. Q. Gao, J. Zheng and W. Zhuang, *J. Phys. Chem. B*, 2013, **117**, 2992–3004.
61 T. Xiao and X. Song, *J. Chem. Phys.*, 2011, **135**, 104104.
62 T. Xiao and X. Song, *J. Chem. Phys.*, 2017, **146**, 124118.
63 W. Hayes, R. Wetzel and R. Freund, *CRC Handbook of Chemistry and Physics*, CRC Press, New York, 2010.
64 A. Perera and T. Urbic, *Phys. A*, 2018, **495**, 393–404.
65 S. H. Lee and J. C. Rasaiah, *J. Phys. Chem.*, 1996, **100**, 1420–1425.
66 A. Vincze, P. Jedlovszky and G. Horvai, *Anal. Sci.*, 2002, **17**, i317–i320.
67 H. J. Berendsen, D. van der Spoel and R. van Drunen, *Comput. Phys. Commun.*, 1995, **91**, 43–56.
68 D. Van Der Spoel, E. Lindahl, B. Hess, G. Groenhof, A. E. Mark and H. J. Berendsen, *J. Comput. Chem.*, 2005, **26**, 1701–1718.
69 S. Nosé, *J. Chem. Phys.*, 1984, **81**, 511–519.
70 W. G. Hoover, *Phys. A*, 1985, **31**, 1695–1697.
71 T. Darden, D. York and L. Pedersen, *J. Chem. Phys.*, 1993, **98**, 10089–10092.
72 S. Miyamoto and P. A. Kollman, *J. Comput. Chem.*, 1992, **13**, 952–962.
73 M. P. Allen and D. J. Tildesley, *Computer simulation of liquids*, Oxford University Press, 1989.
74 W. Kob, C. Donati, S. J. Plimpton, P. H. Poole and S. C. Glotzer, *Phys. Rev. Lett.*, 1997, **79**, 2827–2830.
75 N. Lačević, F. W. Starr, T. Schrøder and S. Glotzer, *J. Chem. Phys.*, 2003, **119**, 7372–7387.
76 S. Karmakar, C. Dasgupta and S. Sastry, *Proc. Natl. Acad. Sci. U. S. A.*, 2009, **106**, 3675–3679.
77 C. Donati, S. Franz, S. C. Glotzer and G. Parisi, *J. Non-Cryst. Solids*, 2002, **307**, 215–224.
78 A. Perera, *Phys. Chem. Chem. Phys.*, 2017, **19**, 1062–1073.
79 K. Binder and W. Kob, *Glassy materials and disordered solids: An introduction to their statistical mechanics*, World Scientific, 2011.
80 Z. Shi, P. G. Debenedetti and F. H. Stillinger, *J. Chem. Phys.*, 2013, **138**, 12A526.
81 D. Jeong, M. Y. Choi, H. J. Kim and Y. Jung, *Phys. Chem. Chem. Phys.*, 2010, **12**, 2001–2010.
82 L. O. Hedges, L. Maibaum, D. Chandler and J. P. Garrahan, *J. Chem. Phys.*, 2007, **127**, 211101.
83 A. Ikeda and K. Miyazaki, *Phys. Rev. Lett.*, 2011, **106**, 015701.
84 L. Xu, F. Mallamace, Z. Yan, F. W. Starr, S. V. Buldyrev and H. E. Stanley, *Nat. Phys.*, 2009, **5**, 565–569.
85 P. Kumar, S. V. Buldyrev, S. R. Becker, P. H. Poole, F. W. Starr and H. E. Stanley, *Proc. Natl. Acad. Sci. U. S. A.*, 2007, **104**, 9575–9579.
86 S. H. Lee and J. C. Rasaiah, *J. Chem. Phys.*, 1994, **101**, 6964–6974.
87 B. Hess, *J. Chem. Phys.*, 2002, **116**, 209–217.
88 S. Murad, *J. Chem. Phys.*, 2011, **134**, 114504.
89 R. Shi and Y. Wang, *J. Phys. Chem. B*, 2013, **117**, 5102–5112.
90 R. Juárez-Maldonado, M. A. Chávez-Rojo, P. E. Ramírez-González, L. Yeomans-Reyna and M. Medina-Noyola, *Phys. Rev. E: Stat., Nonlinear, Soft Matter Phys.*, 2007, **76**, 062502.
91 J. N. Canongia Lopes, M. F. Costa Gomes and A. A. H. Pádua, *J. Phys. Chem. B*, 2006, **110**, 16816–16818.
92 J. P. Hansen and I. R. McDonald, *Theory of Simple Liquids*, Elsevier Science, 1990.
93 E. Flenner and G. Szamel, *Phys. Rev. E: Stat., Nonlinear, Soft Matter Phys.*, 2004, **70**, 052501.
94 F. H. Stillinger Jr., *J. Chem. Phys.*, 1963, **38**, 1486–1494.

